Electronic Supplementary Material (ESI) for Journal of Analytical Atomic Spectrometry.

Electronic Supplementary Information

Increased Sensitivity in Proton-Transfer-Reaction Time-of-Flight Mass Spectrometry by Using a Novel Traveling Wave based Ion-Molecule Reactor

Xing Guo[a], Juan Pu[b], Jianxiong Dai[c], Xin Wang[a], Xinxue Zhang[a], Yanting Yang[c],

Zhongjun Zhao[d*], Yixiang Duan[a, e*]

[a]College of Chemistry and Material Science, Northwest University,

Xi'an 710069, P.R. China;

[b]College of Chemistry, Sichuan University,
Chengdu 610064, P.R. China;
[c]Aliben Science and Technology Company Limited, Chengdu 610064, P.R. China;

[d]School of Mechanical Engineering, [e]Research Center of Analytical Instrumentation,

Sichuan University,

Chengdu 610064, P.R. China;

* Address correspondence to:
Prof. Yixiang Duan, Research Center of Analytical Instrumentation, Northwest University, 1 Xuefu Ave., Xi'an, 710075, P.R. China; E-mail: yduan@nwu.edu.cn.
Associate professor Zhongjun Zhao, School of Mechanical Engineering, Sichuan University, 29 Wangjiang Road, Chengdu 610064, P.R. China; E-mail: zhaozj@scu.edu.cn.

Calibration gas preparation. The corresponding analytical grade reagent (Sinopharm Chemical Reagent Co., Ltd) and relative humidity (RH) 50 percent zero air from cylinder (Winntec specialty gases Co., Ltd) were used to formulate calibration gases with an initial concentration of 4.5×10^{-5} mol/L (acetone, benzene, toluene, xylenes, and styrene). These calibration gases were further diluted in zero air from the cylinder as well. The calibration curve and detection limit were evaluated by a dynamic dilution system as shown in Figure S1. By varying the flow rates of zero air and calibration gas, respectively, which are controlled by two mass flow controller (MFC), the calibration gas could be obtained from 10^4 to 10^6 folds.

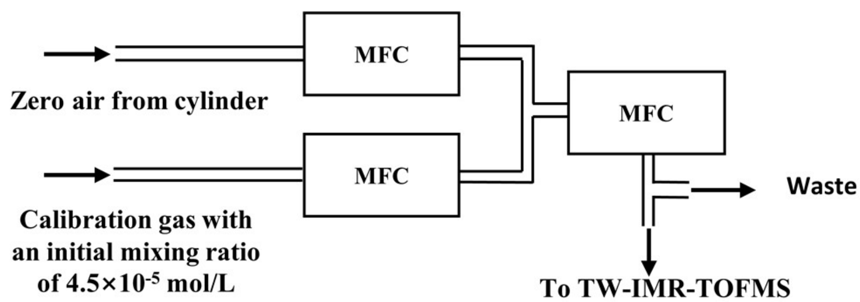

Figure S1. Dynamic calibration gas diluting system.

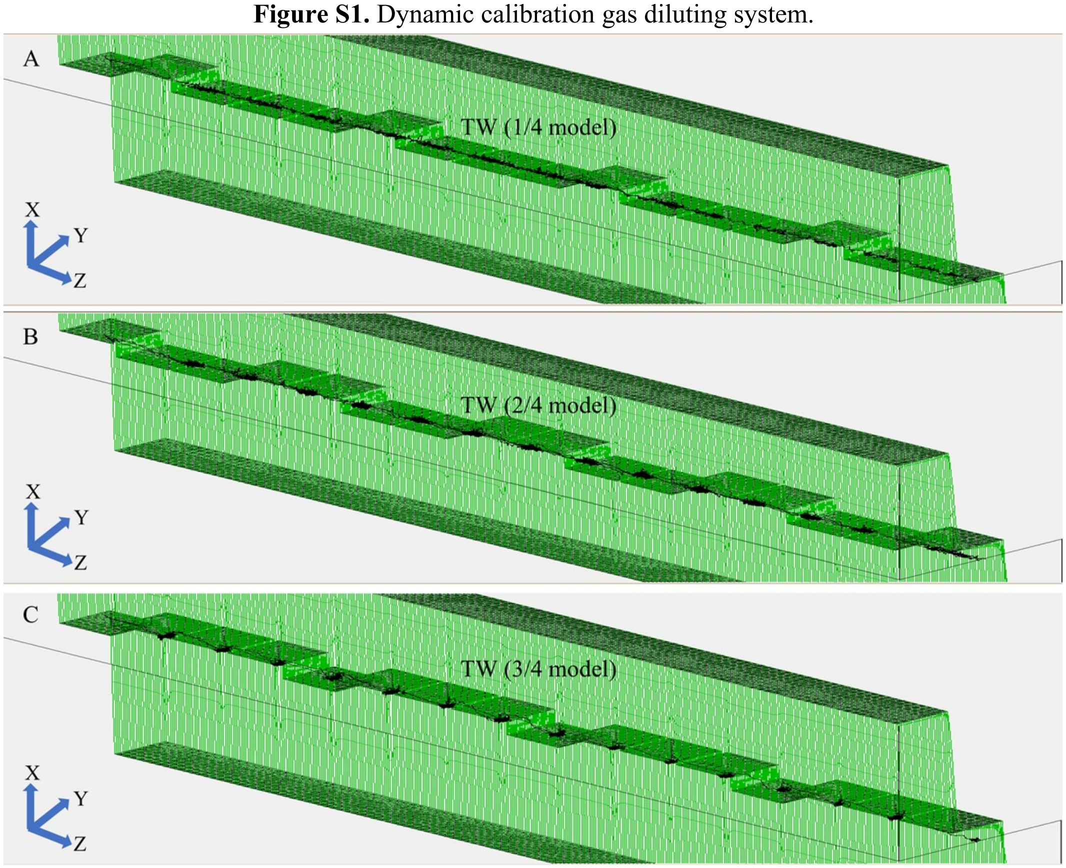

Figure S2. Three traveling wave push modes: (A) 1/4 mode, (B) 2/4 mode, and (C) 3/4 mode;

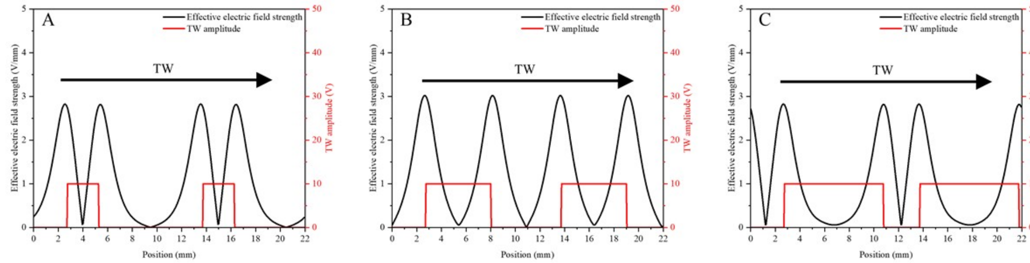

Figure S3. The effective electric field strength generated by 10 V TW amplitude at different axial positions in TW-IMR device under different TW duty cycle modes: (A) 1/4 mode, (B) 2/4 mode, and (C) 3/4 mode;

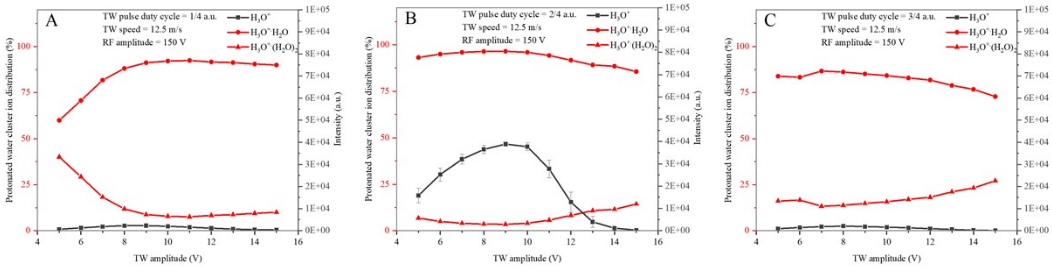

Figure S4. Influences of the TW amplitude upon the relative proportions (red line) of $H_3O^+{\cdot}H_2O$ and $H_3O^+{\cdot}(H_2O)_2$ signal intensities and the selective ion current (SIC) signal intensity of H_3O^+ (black line) under different TW duty cycle modes: (A) 1/4 mode, (B) 2/4 mode, and (C) 3/4 mode; uncertainties were confirmed from the analysis of ten trials.

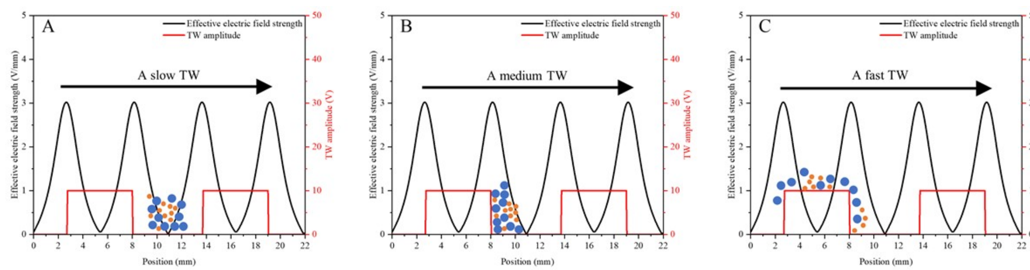

Figure S5. The motion state of ion clusters in the TW electric field at different TW speeds: (A) slow TW, (B) medium TW, and (C) fast TW;

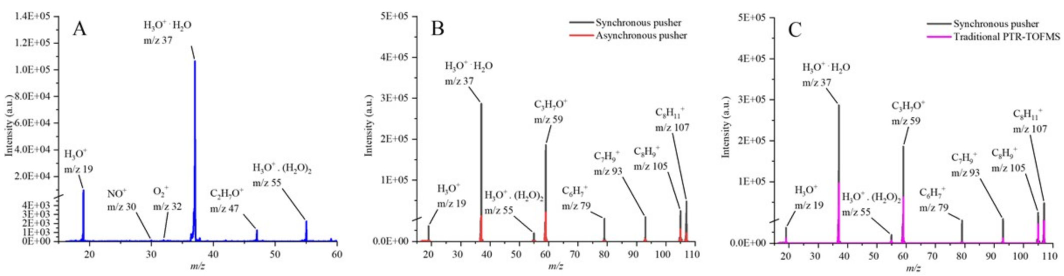

Figure S6. (A) The reagent ion mass spectrum with zero air as blank after parameter optimization; (B) Comparison of mass spectra the synchronous (black line) and asynchronous (red line) modes; (C) Comparison of mass spectra the synchronous mode (black line) and traditional PTR-TOFMS (purple line);